Accepted Manuscript

Ab-initio and experimental study of phase stability of Ti-Nb alloys

J.J. Gutiérrez Moreno, M. Bönisch, N.T. Panagiotopoulos, M. Calin, D.G. Papageorgiou, A. Gebert, J. Eckert, G.A. Evangelakis, Ch.E. Lekka

PII: S0925-8388(16)33712-4

DOI: 10.1016/j.jallcom.2016.11.231

Reference: JALCOM 39728

To appear in: *Journal of Alloys and Compounds*

Received Date: 17 August 2016

Revised Date: 28 October 2016

Accepted Date: 17 November 2016

Please cite this article as: J.J. Gutiérrez Moreno, M. Bönisch, N.T. Panagiotopoulos, M. Calin, D.G. Papageorgiou, A. Gebert, J. Eckert, G.A. Evangelakis, C.E. Lekka, Ab-initio and experimental study of phase stability of Ti-Nb alloys, *Journal of Alloys and Compounds* (2016), doi: 10.1016/j.jallcom.2016.11.231.

Phase stability of β Ti-based alloys suitable for biomedical applications

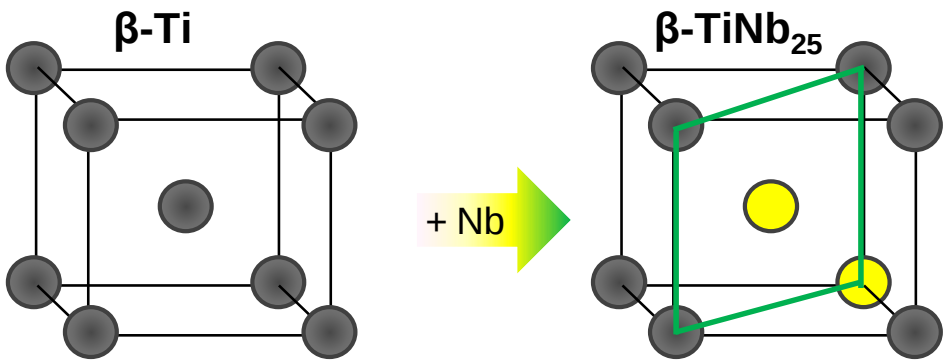

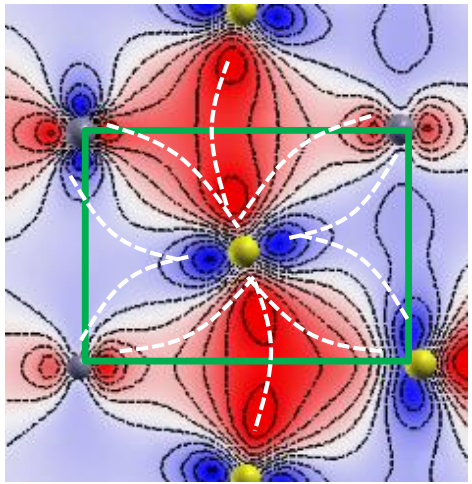

Unstable β-Ti
with desired low young moduli

Stable β-$TiNb_{25}$ alloy due to the
directional covalent-like bonding

Ab-initio and experimental study of phase stability of Ti-Nb alloys

J.J. Gutiérrez Moreno[a,b], M. Bönisch[c,d], N. T. Panagiotopoulos[e,f,g], M. Calin[c], D.G. Papageorgiou[a], A. Gebert[c], J. Eckert[c,h,i], G.A.Evangelakis[e], Ch.E. Lekka[a*]

a Department of Materials Science & Engineering, University of Ioannina, Greece

b Tyndall National Institute, University College Cork, Ireland

c Institute of Complex Materials, IFW Dresden, P.O. Box 270116, D-01171 Dresden, Germany

d Institute of Structural Physics, Technische Universität Dresden, Haeckelstraße 3, D-01069 Dresden, Germany

e Department of Physics, University of Ioannina, Greece

f Univ. Grenoble Alpes, SIMAP, F-38000 Grenoble, France

g CNRS, SIMAP, F-38000 Grenoble, France

h Erich Schmid Institute of Materials Science, Austrian Academy of Sciences (ÖAW), Jahnstraße 12, A-8700 Leoben, Austria

i Department Materials Physics, Montanuniversität Leoben, Jahnstraße 12, A-8700 Leoben, Austria

Keywords: Biomaterials, titanium alloys, phase stability

Abstract

A systematic theoretical and experimental study concerning the crystallographic structure and electronic properties of Ti-xNb (x< 50 at%) alloys is presented, aiming to enlighten the electronic origins of the β-phase stability which is of high interest for the development of novel β stabilized

Ti-based alloys for biomedical applications. Both quantum-mechanical calculations and X-ray diffraction found several structural phases depending on Nb concentration. The ab-initio total energy results reveal that at low Nb contents the α´ and ω phases are favoured while at Nb content > 18.75 at% the β-phase is favoured against all other crystallographic structures in line with the experimental results. Interestingly, at high Nb content the α´ and ω hexagonal phases become unstable due to the electronic band filling close to the Fermi level E_F, which is mainly due to Nb-p and Ti-d antibonding hybridizations. On the contrary, in the cubic β-Ti-25Nb (at%) the depletion of the occupied electronic states at the E_F occurs mainly due to Nb-d and Ti-d bonding interactions, resulting in a stable β-TiNb structure. These data could enlighten the electronic origin of the Ti-Nb phase stability, thus, may contribute to the design of β stabilized low moduli Ti-based alloys suitable for load-bearing biomedical applications.

1. Introduction

Ti-based alloys are dominating as metallic biomaterials and in this role are central to the well-being and quality of life of a large part of the human population. Since the 1950s Ti-6Al-4V (wt.%) is the most conventional alloy for medical bone-replacing and supporting use due to its good workability, heat treatability and large strength compared to steels or Co-Cr alloys [1, 2]. However, compatibility concerns in terms of biological safety of V and Al [3, 4] and mechanical properties [5, 6] have motivated extensive efforts since the 90ies to develop β-stabilized Ti-based alloys without harmful elements and reduced Young's modulus. Due to these efforts this class of alloys and in particular Ti-Nb-based, Ti-Ta-based and Ti-Zr-based alloys are emerging as promising materials for load-bearing as well as for functional biomedical implant components [1, 2, 5].

The strongest attention was and is still given to β-phase Ti-Nb-based alloys [**1, 7**, **8**]. The high attractiveness of Ti-Nb alloys is based on their superior combination of low elastic moduli [**9**, **10**], high corrosion resistance [**11, 12**] and minimal cytoxicity [**13, 14**], together with their superelastic and shape memory features [**8, 15, 16**]. Several phases (including α, β, α″ and ω) may coexist in Ti-Nb alloys, depending on the Nb concentration, which decisively influence their mechanical and functional properties, as has been suggested in previous works [**5, 9**]. Nb is a β-stabilizer and, therefore, the body centered cubic (bcc) β-phase is retained at room temperature (RT) by quenching for compositions above about Ti-22.5Nb (at%). For Nb-leaner compositions, the phase transition pathway from the hcp α-phase to into the bcc β-phase gives rise to the α″ orthorhombic phase [**17, 18**]. The suitability of Ti-Nb alloys for some task heavily depends on the composition, microstructural design and processing. Appropriate selection of composition and thermo(mechanical) processing allows tailoring of the mechanical and functional properties for biomedical applications [**4**, **5**, **19**-**21**].

This behavior is directly related to the instability of pure β-Ti at ambient conditions, which is correlated with its elastic instability (negative values of the tetragonal shear modulus C′) [**22, 23**]. For cubic d transition metals and alloys, C′ is associated with the energy difference between the face centered cubic (fcc) and bcc phases, while the stability of the fcc, hexagonal close packed (hcp) and bcc structures is linked to the electronic band filling and the number of d-electrons and the shape of their electronic density of states (EDOS) [**22**]. In particular, the stability of the β-Ti phase is attributed to the increase of the number of d-electrons due to charge transfer from the s and p electrons upon pressure [**24, 25**] or upon alloying with V, Nb, Ta, Mo, and W [**26, 27**] where a critical number of 4.24 valence electrons per atom (e/a) was introduced [**26**] as a convenient predictive criterion. Tailoring C’ and e/a allows obtaining a unique combination of

very low elastic modulus and large elastic strain together with high mechanical strength and large deformability as demonstrated by the “Gum metal” alloy family [26].

In addition, due to the d-electrons, the β-phase elements may exhibit strong directional covalent bonds [**28**]. Covalent bonding was also suggested in the ω–phase of Ti, Zr, Hf [**23**]. Further theoretical studies introduced the Bond order (Bo) as a measure of the strength of the covalent bonding, while another theoretical model combines the Bo with the highest occupied molecular orbital centered upon the alloying atom and the resulting absolute- energy value as a measure of the ionization potential of this atom in the corresponding system [**29**]. Both methodologies try to correlate the electronic properties of the Ti-based alloy with the experimentally observed low elastic modulus and shape memory characteristic and provided guidelines for the design of new alloys.

Although during the last years there has been a lot of attention on the Ti-Nb alloys, investigations concerning the whole set of experimentally observed phases (α’, β, α″ and ω) are rare. Most of the studies, especially the theoretical ones, have been focused mainly on the electronic properties and the stability of one or two of the four phases, or on selected alloy compositions. A detailed study of the crystallographic structures and electronic characteristics, combining theoretical calculations with experiments, is lacking.

In this work, we present results from a systematic study of several Ti-Nb alloys covering a large Nb concentration range from 0 at% to 50 at%, combining both experimental and theoretical data. The α′, β, α″ and ω phases observed in our experimental Ti-Nb samples (in both bulk and thin film forms) were studied by ab-initio calculations seeking for the electronic origin of their formation, as well as their stabilities. The lattice parameters and the EDOS were obtained for all phases and Nb concentrations, in order to uncover their influence in the resulting poly-crystalline alloys.

2. Experimental details

Ingots of binary Ti-Nb alloys with Nb content between 4.9 at% and 29.3 at% were prepared by arc melting the unalloyed elements (purity 99.7% or higher) in Ar atmosphere. To ensure complete melting of the elemental Ti and Nb each ingot was re-melted for at least 5 times. Subsequently, the ingots were cast into rods by cold-crucible casting using a water-cooled Cu crucible and a Cu mold 10 mm in diameter. The Nb and O contents of the cast alloys were measured by inductively coupled optical emission spectroscopy and carrier hot gas extraction; the corresponding values are reported in [**17**]. In order to prepare a chemically uniform state the as-cast rods were subjected to a homogenization treatment followed by water quenching (HQ). Therefore, the rods were encapsulated in quartz tubes under 150 mbar Ar and homogenized in the single β-phase field at 1000°C for 24 h. In order to suppress diffusional processes leading to local changes in the compositions during cooling the rods were quenched into water. Slices of these rods were mechanically thinned to below 100 µm by grinding with SiC paper for X-ray diffraction (XRD), which was performed in transmission geometry at RT in a STOE STADI P diffractometer operated with Mo-Kα1 radiation (λ = 7.093 Å). The scattering angle is reported in terms of the wavevector transfer $Q = (4\pi \cdot \sin\theta)/\lambda$. Phase analysis was carried out and the lattice parameters of the identified phases were determined by Rietveld refinement using FullProf [**30**]. Details of the refinements are given in [**17**]. HQ samples for light microscopy (LM) were mechanically ground, polished and etched with an aqueous solution containing 2 vol.% HF and 6.5 vol.% HNO_3.

Binary Ti-Nb films were deposited on commercial, Czochralski-grown, n-type Si(001) cleaned in ultrasound acetone and methanol bath in sequence, followed by dip in Hydrofluoric acid (HF),

rinse off by dionized water and then dried under high pressure flow of high purity Nitrogen (purity 99.999%). The deposition was performed by dual-cathode confocal magnetron sputtering using high purity Ti (purity 99.995%) and Nb (purity 99.8%) magnetron targets in a high vacuum chamber (base pressure of $5x10^{-6}$ mbar). As sputtering gas we used high purity Ar (purity 99.999%), which was leaked in the deposition chamber achieving working pressure of $4x10^{-2}$ mbar. The applied power to the magnetron guns was fixed at 80W RF and 15W or 30W DC for the Ti and the Nb targets, respectively. The compositions of the grown samples were determined by energy dispersive X-ray spectroscopy (EDS) in a JEOL 5600 scanning electron microscope coupled to an Oxford Link ISIS L300 detector, while grazing incidence XRD measurements were performed in a Bruker D8-Advance diffractometer with Cu-Ka radiation for the evaluation of the crystal structure of the grown Ti-based films.

3. Computational Method

We performed quantum mechanical calculations based on the density functional theory using the linearized augmented plane wave method within the WIEN2k software [**31**]. This method expands the Kohn–Sham atomic-like orbitals inside the atomic muffin tin (MT) spheres and the plane waves in the interstitial region. The MT radii were taken 2.5 a.u. for both Ti and Nb atoms. The calculations were performed with the exchange correlation functional treated within the generalized gradient approximation GGA (PBE96) [**32**]. In order to simulate the α′, β, α″ and ω phases we used several unit cell configurations with respect to the Nb concentrations and sampling of the Brillouin zone. In particular as presented in Table 1, the α'-Ti has space group P63/mmc (No. 194) with 2 basis atoms placed at the Wyckoff positions (1/3, 2/3, 1/4) and (2/3, 1/3, 1/4); the ω-Ti has space group P6/mmm (No. 191) and 3 basis atoms were at (0, 0, 0), (1/3, 2/3, 1/2) and (2/3, 1/3, 1/2); the α"-Ti with space group Cmcm (No. 63) was constructed using 4

atoms situated at (0, 0, 0), (0, y, 0), (1/2, 1/2, 0) and (0, 1/2+y, 1/2) [50], the y parameter denotes the shuffle and it was set to 0.1 that is the typical value for the Ti-Nb alloys [51]; and the β-Ti with space group $Im\bar{3}m$ (No. 229) is defined by one atom located at the origin. For the pure Ti phases 2925, 1098, 2736 and 1540 k-points were used to sample the α'-Ti, ω-Ti, α''-Ti and β-Ti, respectively. Using these space groups and the corresponding lattice vectors and basis atoms supercells were created having up to 32 atoms (β Ti-9Nb(at%), 242 (12×12×6) k-points) in order to simulate several Ti-Nb compositions as denoted in Table I. Due to the different number of the α', ω, α'' and β basis atoms it is impossible in Ti-Nb to simulate exactly the same Nb composition for all phases. The k-point sampling was chosen large enough to reach convergence and scaled upon the number of atoms, for example, for the 32 atoms unit cell a 12×12×6 (242) k-point mesh was employed.

Aiming to identify the more stable atomic conformation of each phase, several different occupations of Nb ions within each Ti structure especially for the high Nb compositions. In [46] we have found that the critical point for energetically favoured configuration depends in the appearance of Nb-Nb First neighbours (FN), Second neighbours (SN) or Third neighbours (TN) and it is related not only with the Nb composition but also with the coordination number of each phase. In particular, for small Nb (<8at%) contents (Nb-Nb are third neighbours and the hexagonal structures are preferred), the Ti-8,33at% Nb composition stands for the existence of one Nb atom among 12 Ti first neighbours having mainly Nb-Nb SN (stand mainly for the orthorhombic phase) while for higher Nb compositions the existence of Nb-Nb FN emerges that stabilizes the β-phase (obvious since Nb prefers the β-phase and the Nb-Nb FN bonding hybridizations enhancing the critical corner-central atom bonding of the β-phase) [46]. In the Fig.1 we present an example for the different occupations of Nb ions within Ti structures for the: a) Ti-18.75at%Nb were the Nb-Nb SN configurations are found to be favoured while the b) Ti-

25at%Nb the Nb-Nb FN preference emerges. The DEtotvalues/ eV/atom are given relatively to the energetically favored phase for each Nb composition in parenthesis while for the Ti-18,75at%Nb case the α″ phase is unflavoured to the β-phase by 0,047 eV/atom as depicted in Fig.4. Finally, for the smallest compositions like Ti-6.25at%Nb our ab initio WIEN2k unit cell consist of 16 atoms having 15 Ti atoms and 1 Nb atom resulting equivalent positions for the doping element.

4. Results and discussion

4.1 **Phases identified by XRD**

The XRD patterns and typical microstructures of the bulk HQ Ti-Nb alloys are shown in Fig. 2. The main structural constituent in these alloys is either α', α" or β. In addition, in all martensitic alloys minor amounts of ω and/or retained β are present according to XRD. In Nb-lean alloys containing less than 9 at% Nb mainly hexagonal martensite α' was found. Alloys with Nb contents from 9 at% to 20.4 at% consist primarily of the orthorhombic martensite α''. These observations are in excellent agreement with the literature [**8, 18, 35, 40, 41**]. Besides α'', alloys containing 22.4 at% Nb and more contained increasing amounts of retained β that did not transform into martensite by quenching. Lower limits for the presence of retained β ranging between 17−20 at% Nb were reported in the literature as discussed in [**17**]. The scatter of these values may result from the presence of minor amounts of athermal and/or isothermal ω in these alloys. Bragg-reflections of β and ω in 1-dimensional diffractograms are subject to severe overlapping [**33**] and if reflections unique to ω, such as $(0001)_\omega$,$\{11\bar{2}1\}_\omega$ or $(0002)_\omega$, are not excited or absent because of its low volume fraction, the remaining reflections may be easily interpreted in terms of β instead of ω. For Nb contents higher than 24.9 at% no secondary phases were detected in β. The composition limits within which α'' is found corresponding to a valence electron per atom ratio of e/a = 4.08 (lower limit) and e/a = 4.25 (upper limit) [24].

Fig. 3 depicts the lattice parameters obtained from our XRD measurement and our ab-initio total energy minima for various Nb contents for the α′, ω, α″ and β phases. The diagram compares these values with theoretical values from the literature and the experimental lattice parameters corresponding to the diffractograms in Fig. 2 and literature sources [**17**, **34-42**]. The experimental lattice parameters of α′, α″ and β obtained from Fig. 1 below 25 at% Nb are reproduced from [**17**].

Depending on the crystal symmetry of the identified phases, up to three different lattice parameters exist. For the hexagonal α′ phase, Fig. 3a, the ab-initio data show that the lattice parameter $a_{\alpha'}$ decreases, while $c_{\alpha'}$ increases with increasing Nb content almost linearly. In addition, we find that the α′ volume increases and the theoretical results are comparable with the experimental data [**17**].

In Fig. 3b, the ab-initio results of the lattice parameters of ω are shown. In addition, the XRD data are also shown in this figure using the largest and smallest lattice parameters of ω one obtains if the low intensity reflections in Fig. 1 (e.g. located at Q=2.7 $Å^{-1}$ and Q=3.8 $Å^{-1}$) are attributed to ω. A very good agreement is found between the ab-initio and the experimentally determined ranges of the ω lattice parameters. In the ω-phase the lattice parameter a_ω increases and is larger than c_ω which decreases upon Nb enrichment, resulting in an enlargement of the ω volume similarly to the case of α′. It should be noted that although different, a similar increasing behavior of the ω phase's a_ω lattice parameter and the α′ phase's $c_{\alpha'}$ lattice parameters expected due to the orientation relation between the ω and α′ unit cells ($(01\bar{1}1)_\omega$ is parallel to $(0001)_{\alpha'}$).

In the orthorhombic α″ phase, we can distinguish three independent lattice parameters ($a_{\alpha''}$, $b_{\alpha''}$ and $c_{\alpha''}$) that are presented in Fig. 3c along with several experimental and theoretical data. The XRD data available in the literature agree very well [**17, 18, 34, 35-37, 39-42**] while the small deviations of our ab-initio values are related to the several approximations introduced in our first

principles calculations. Some examples of the limitations in our theoretical approach are the absence of temperature and pressure, the small unit cell sizes (up to 32 atoms) or the multitude of available relative positions that substitutional Nb atoms may occupy within the Ti tetragonal box. Nevertheless, both theoretical and experimental data follow, in general, the same trend as the Nb content increases. The $a_{\alpha''}$ lattice parameter increases with the gradual Nb replacement while $b_{\alpha''}$ and $c_{\alpha''}$ are reduced, as seen in Fig. 3c. Despite this difference, the volume of the α″ unit cell increases upon Nb substitution according to the ab-initio data, in line with the α′ and ω phases.

Finally, in Fig. 3d, we present the increasing behavior of lattice parameter of the β-phase as a function of Nb. As in the case of ω, this figure also includes the largest and smallest experimental lattice parameters of β one obtains if the low intensity reflections are attributed to the β phase. We observe that our Ti-Nb XRD data for both bulk and thin films agree with the available experimental ones [**17**, **26, 34, 35-37, 42**]. Meanwhile our ab-initio calculations are close to other theoretical results [**43, 26**] and to the β-Ti-30Nb (at%) single crystal value [**34**] due to the similarity of the unit cells, in contrast with the polycrystalline structure of the arc melted alloys. Also in this case, our calculations underestimate the experimental results because of the approximations of the ab-initio calculations and show an increasing trend of the lattice parameter of β upon Nb addition, in agreement with the experimental data sets in [**7**, **17**].

4.2 Crystallographic structure versus electronic properties by theoretical calculations

The experimentally observed α′, β, α″ and ω Ti-Nb phases were studied systematically by means of ab-initio calculations aiming to reveal the relation between structure, phase stability and electronic properties. In Fig. 4 we present the total energy difference (DEtot) and the EDOS for several Ti-Nb alloys and for pure Ti. The DEtot is given as a function of the unit cell volume under hydrostatic pressure and the EDOS correspond to the lowest energy configuration for each

phase. It should be noted that all DEtotvalues are given relatively to the energetically favoured phase for each Nb composition, while in the EDOS the Fermi level (E_F) is set to zero.

Starting with pure Ti, we found that the β-Ti is clearly least energetically favoured among α′, β, α″ and ω, while the hexagonal α′-Ti and ω-Ti exhibit almost equal DEtot values, in line with previous theoretical [**43**] and experimental [**44**] results. Interestingly, the DEtot between the β-Ti and the α′-Ti is correlated with the corresponding EDOS's lowest electron occupation close to E_F, Fig. 4. The lowest α′-Ti's total energy against the β-Ti was previously theoretically found for Ti, Zr and Hf and it was attributed to the shape of the EDOS, in particular to the lowest d electron occupation at E_F [40]. Ti-6.25Nb (at%) exhibits similar characteristics to pure Ti, yielding the β-Ti-6.25Nb (at%) energetically unfavoured and showing the highest electron occupation at E_F against the other phases. The α″-Ti-12.5Nb (at%) DEtot is almost equal to those of α′-Ti-12.5Nb (at%) and ω-Ti-12.5Nb (at%) hexagonal structures, revealing similar electronic occupation at E_F denoting the gradual stability improvement of the α″ phase, in line with our experimental observations and previous experimental works [**8, 26, 37, 45**]. As the amount of Nb substitutions increases, the β phase becomes energetically favoured for Ti-18.5Nb (at%) and Nb richer compositions by almost 0.05eV/atom. Nevertheless, for this case the total EDOS at the fermi level does not saw the lowest occupation for the β-phase and therefore for high Nb compositions the full energy length of EDOS (from -4eV up to fermi) should be investigated as depicted as in the following Fig. 5a. For Ti-50Nb (at%), α′ is expected to be totally unstable due the highest DEtot and the filling of the EDOS at E_F, compared to the pure α′-Ti. Similarly, the ω-Ti-50Nb (at%) and α″-Ti-50Nb (at%) phases exhibit enhanced occupancy of the d-bands between -0.5eV and E_F compared to Ti-6.25Nb (at%), while the β-$TiNb_{6.25}$ EDOS peak at E_F decreases, denoting improved stability of β in Ti-50Nb (at%). Although the current Total energy and EDOS results refer to the perfect CsCl β Ti-50at%Nb and not in the solid solution β-phase that is experimental

observed for high Nb contents they offer the corresponding preference against an orthorhombic or a hexagonal type structure while for the β Ti-18.75at%Nb and β Ti-25at%Nb β solid solution phase was simulated and the configuration with Nb-Nb first neighbours was found energetically favoured compared to the Nb-Nb second neighbour configuration and to the other phase as presented in Fig.1 and Fig.4 [46].

The EDOS alterations in α′, β, α″ and ω upon Nb substitution are presented in detail in Fig. 5a where besides the total EDOS the partial electronic density of states (PEDOS) of Ti and Nb are also shown. Each row corresponds to the EDOS and PEDOS of one of the four phases. The EDOS of α′ exhibits a local minimum at around -0.5eV below E_F (indicated by an arrow) which gradually changes upon Nb substitution. Interestingly, for a Nb content of 25 at% a peak emerges inside this EDOS minimum denoting instability of this phase at high Nb content, in agreement with our experimental data (Fig. 2). This peak is mainly due to the Nb-p PEDOS (Fig. 5a) while, interestingly, the presence of Nb p electrons at around -0.5eV introduce mostly antibonding or non-bonding sites with most of the first neighboring Ti d electrons. These bonding and antibonding features of the Nb p-electrons with the d-electrons of the Ti neighbours are presented in Fig. 4b, for the corresponding wavefunction of the -0.5eV energy peak, inside the $(0001)_{\alpha'}$ plane on which the shear transition from α' phase to α'' or βand vice versa takes place. From blue to red colour scale the positive/negative charge values of the wavefunction are denoted that reveal the bonding (similar colour) or antibonding (different colour) hybridizations between the atoms. In particular, two weak directional bonds (shown by dashed blue lines) are formed between the blue lobe of the Nb p electrons and the blue d electron lobes of the Ti_6 and the Ti_1 atoms. Meanwhile antibonding or non-bonding features are found between the Nb p orbital and the other neighboring Ti (named Ti_2, Ti_3, Ti_4 and Ti_5) d electrons' lobes. In particular, the Nb p electron's red lobe (negative charge of the wavefunction) has a different charge sign than the Ti_2, Ti_3 and Ti_4

d blue electrons' lobes (positive charge of the wavefunction), thus indicating that these non-bonding or even antibonding features in the $(0001)_{\alpha'}$ plane may destabilize the α′-Ti-25Nb (at%) towards the α", along a transformation pathway similar to NiTi [48], or β phases following the corresponding Burgers orientation relationships [49].

Similar behavior in the EDOS and wavefunction characteristics were also found in the ω phase, in which the EDOS (shown in the second row Fig. 5a) suggests that as the Nb amount increases the electronic states are depleted (green arrow in the Nb PEDOS's at -3.0eV), while the gradual increase of the EDOS around -0.5eV is mainly due to Nb pd-PEDOS and Ti d-PEDOS. Moreover, in line with α′-Ti-25Nb (at%) the presence of Nb p electrons close to E_F introduces antibonding features with the d electrons of the Ti first neighbouring atoms for all available Nb sites (inside the honeycomb or hexagonal ω sub-lattice) [**46**]. The third row in Fig. 4a shows the EDOS and PEDOS of the α″ phase. The α″-Ti-6.25Nb (at%) is unstable since there is no local EDOS minimum at E_F, while as the Nb substitution increases the EDOS decreases and low values emerge for α″-Ti-25Nb (at%) denoting stability of this phase [**22, 23**]. Similarly, to the α″ phase, the β-Ti-6.25Nb (at%) is unstable, while for higher Nb compositions the electronic states are shifted towards lower energies, especially for the broad band below -1eV, while the EDOS at E_F exhibits a local minimum. This connection between the EDOS features and the β-phase stability has been also recently proofed in ternary Ti-Nb alloys containing doping elements such Sn [**47**] or In [**21**]. These features are due to the strong Ti d - Nb d electron bonding hybridizations as depicted in Fig. 5c for the β-Ti-25Nb (at%) $(110)_\beta$ plane which appear even at the -3.5eV well localized energy state very far from E_F. In particular, the red lobes of the Nb_1d electron are bonded to the first Nb_3 and second $Nb_{2,4}$ neighbouring atoms red lobes forming strong directional σ covalent-like bonds (denoted by the dashed white lines originating from the Nb_1 atom inside the red negatively charged contour area), while the $Ti_{1,2,3}$ first neighbours also

participate. Interestingly the Nb_1 blue d electron lobes are also hybridized with the blue d lobes of the first neighbouring $Ti_{1,2,3}$ and Nb_3 atoms, thereby strengthening the bonds and the stability of the structure. These bonding characteristics uncover the electronic origin of the β phase stability against the α' phase for aNb content of 25at%.

5. Conclusions

In this work, we present experimental and theoretical results regarding the crystallographic structure and electronic properties of Ti-Nb phases. We found that upon increasing the Nb content several phases may coexist, starting with the hexagonal (α′ and ω) at low Nb amounts, followed by the orthorhombic martensite (α″) at intermediate Nb content and the cubic β phase for the highest Nb concentration. Both experimental and theoretical results agree that the volume of the unit cells of α′ and β expands with increasing Nb content. The ab-initio total energy difference results for low Nb contents favor the α´ and ω phases, while the β-Ti-18.5Nb (at%) is found to be stable against all other phases, in line with the experimental results. In addition, we found that Nb enrichment results in the enhancement of the total number of d-electrons and p-semi core electrons. Interestingly, this effect, in conjunction with the Nb-Ti hybridizations, is responsible for the depletion of the occupied electronic states at E_F, which characterize the β-phase of Ti, thus leading to a stable β-Ti-Nb structure at high Nb content. On the contrary, the Nb-Ti antibonding features close to E_F are related with the corresponding band filling and the instability of the hexagonal α' and ω phases upon Nb substitution. These theoretical predictions are in agreement with the experimental results according to which the Ti-Nb system exhibits a variety of phases (including α´, β, α″) depending on the Nb concentration. These results could be of use for the design of Ti-based alloys suitable for biomedical applications such as load-bearing and/or functional implants.

Acknowledgments: This work was supported by the BioTiNet ITN (No. 264635) FP7 Marie Curie project and further benefited from funding by the German Science Foundation within SFB/Transregio 79.

References

(1) Niinomi, M. Metals for Biomedical Devices. CRC Press (2010).

(2) Niinomi, M.; Hattori, T.; Kasuga, T.; Fukui, H. Titanium and Its Alloys, Encyclopedia of Biomaterials and Biomedical Engineering (2006).

(3) Wang, K. The use of titanium for medical applications in the USA. Materials Science and Engineering: A 213, 1–2 (1996) 134–137.

(4) Biesiekierski, A.; Wang, J.; Gepreel, M.A.H. Wen, C. A new look at biomedical Ti-based shape memory alloys. Acta Biomaterialia 8(5) (2012) 1661–1669.

(5) Niinomi, M. Mechanical biocompatibilities of titanium alloys for biomedical applications. Journal of the Mechanical Behavior of Biomedical Materials 1 (2008) 30–42.

(6) Hanada, S.; Matsumoto, H.; Watanabe, S. Mechanical compatibility of titanium implants in hard tissues. International Congress Series 1284 (2005) 239–247.

(7) Kim, H.Y.; Miyazaki, S. Martensitic Transformation and Superelastic Properties of Ti-Nb Base Alloys. Materials Transactions 56(5) (2015) 625–634.

(8) Kim, H.Y.; Ikehara, Y.; Kim, J.I.; Hosoda, H.; Miyazaki, S. Martensitic transformation, shape memory effect and superelasticity of Ti–Nb binary alloys. Acta Materialia 54 (2006) 2419–2429.

(9) Ozaki, T.; Matsumoto, H.; Watanabe, S.; Hanada, S. Beta Ti alloys with low Young's modulus. Materials Transactions 45 (2004) 2776–2779.

(10) Bönisch, M.; Calin, M.; van Humbeeck, J.; Skrotzki, W.; Eckert, J. Factors influencing the elastic moduli, reversible strains and hysteresis loops in martensitic Ti-Nb alloys. Materials Science and Engineering C 48(0) (2015) 511–520.

(11) Williams, R.L.; Brown, S.; Merritt, K. Electrochemical studies on the influence of proteins on the corrosion of implant alloys. Biomaterials 9 (1988) 181–186.

(12) Schutz, R.W. Environmental behavior of beta titanium alloys. Titanium Alloy Overview 46-7 (1994) 24-29.

(13) Kuroda, M.; Niinomi, M.; Morinaga, Kato, Y.; Yashiro. Design and mechanical properties of new β type titanium alloys for implant materials. Materials Sciences and Engineering: A 243 (1998) 244–249.

(14) Niinomi, M. Development of β Type Titanium Alloys for Impant Materials. Materia Japan 37(1998) 843–846.

(15) Miyazaki, S.; Kim, HY.; Hosoda, H. Development and characterization of Ni-free Ti-base shape memory and superelastic alloys. Materials Science and Engineering: A (2006) 438–440:18–24.

(16) Hosoda, H.; Fukui, Y.; Inamura, T.; Wakashima, K.; Miyazaki, S.; Inoue, K. Mechanical properties of Ti-based shape memory alloys. Materials Science Forum (2003) 426–432:3121–6.

(17) Bönisch, M.; Calin, M.; Giebeler, L.; Helth, A.; Gebert, A.; Skrotzki, W.; Eckert, J. Composition-dependent magnitude of atomic shuffles in Ti-Nb martensites. Journal of Applied Crystallography 47(4) (2014) 1374–1379.

(18) Banumathy, S.; Mandal, R. K.; Singh, A.K. Structure of orthorhombic martensitic phase in binary Ti–Nb alloys. Journal of Applied Physics 106 (2009) 093518

(19) Banerjee, R.; Nag, S.; Fraser, H.L. A novel combinatorial approach to the development of beta titanium alloys for orthopaedic implants, Materials Science and Engineering C 25 (2005) 282–289.

(20) Geetha, M.; Singh, A.K.; Asokamani, R.; Gogia, A.K. Ti-based biomaterials, the ultimate choice for orthopaedic implants - a review. Progress in Materials Science 54 (2009) 397–425.

(21) Calin, M.; Helth, A.; Gutiérrez Moreno, J.J.; Bönisch, M.; Brackmann, V.; Giebeler, L.; Gemming, T.; Lekka, Ch.; Gebert, A.; Schnettler, R.; Eckert, J. Elastic softening of β-type Ti-Nb alloys by indium (In) additions. Journal of the Mechanical Behavior of Biomedical Materials 39 (2014) 162-174.

(22) Söderlind, P.; Eriksson, O.; Wills, J. M.; Boring, A. M. Theory of elastic constants of cubic transition metals and alloys. Physical Review B 48 (1993) 5844-5851

(23) Ahuja, R.; Wills, J. M.; Johansson, B.; Eriksson, O. Crystal structures of Ti, Zr, and Hf under compression: Theory. Physical Review B 48 (1993) 16269-16279.

(24) Hu, Q.M.; Lu, S.; Yang, R. Elastic stability of β-Ti under pressure calculated using a first-principles plane-wave pseudopotential method. Physical Review B 78 (2008) 052102 – 052106.

(25) Zhang, S.; Zhu, Y.; Zhang, X.; Zhang, S.; Qi, L.; Ripping, L. First-principles study on the structural stabilities, electronic and elastic properties for zirconium under pressure, Computational Materials Science 50 (2010) 179-183.

(26) Ikehata, H.; Nagasako, N.; Furuta, T.; Fukumoto, A.; Miwa, K.; Saito, T. First-principles calculations for development of low elastic modulus Ti alloys. Physical Review B 70 (2004) 174113-174121

(27) Raabe, D.; Sander, B.; Friak, M.; Ma, D.; Neugebauer, J. Theory-guided bottom-up design of ´beta-titanium alloys as biomaterials based on first principles calculations: Theory and experiments. Acta Materialia 55 (2007) 4475–4487.

(28) Lee, S.; Hoffmann, R. Bcc and Fcc Transition Metals and Alloys: A Central Role for the Jahn-Teller Effect in Explaining Their Ideal and Distorted Structures, Journal of the American Chemical Society 124 (2002) 4811-4823.

(29) Abdel-Hady, M.; Hinoshita, K.; Morinaga, M. General approach to phase stability and elastic properties of b-type Ti-alloys using electronic parameters, Scripta Materialia 55 (2006) 477–480.

(30) Rodriguez Carvajal, J. FullProf2.k (version 5.60): Rietveld, profile matching & integrated intensity refinement of X-ray and/or neutron data, ILL.

(31) Blaha, P.; Schwarz, K.; Madsen, G. K. H.; Kuasnicka, D.; Luitz, J. WIEN2k, Augmented Plane Wave Local Orbitals Program for Calculating Crystal Properties. Vienna University of Technology (2001).

(32) Perdew, J.P.; Burke, K.; Ernzerhoff, M. Generalized Gradient Approximation Made Simple. Physics Review Letters 77 (1996) 3865-3868.

(33) Panigrahi, A.; Bönisch, M.; Waitz, T.; Schafler, E.; Calin, M.; Eckert, J.; Skrotzki, Zehetbauer, M. Phase transformations and mechanical properties of biocompatible Ti-16.1Nb processed by severe plastic deformation. Journal of Alloys and Compounds 628 (2015) 434-441.

(34) Hermann, R.; Hermann, H.; Calin, M.; Buechner, B.; Eckert, J. Elastic constants of single crystalline beta-Ti70Nb30. Scripta Materialia 66 (2012) 198-201.

(35) Ahmed T.; Rack H.J. Martensitic transformations in Ti-(16-26 at %) Nb alloys. Journal of Materials Science 31 (1996) 4267-4276.

(36) Kim, H.Y.; Ikehara, Y.; Kim, J.I.; Hosoda, H.; Miyazaki, S. Martensitic transformation, shape memory effect and superelasticity of Ti–Nb binary alloys. Acta Materialia 54 (2006) 2419–2429.

(37) Prabha, A.J.; Raju, S.; Jeyaganesh, B.; Rai, A.K.; Behera, M.; Vijayalakshmi, M.; Paneerselvam, G.; Johnson, I. Thermodynamics of α"-β phase transformation and heat capacity measurements in Ti–15 at% Nb alloy. Physica B 406 (2011) 4200–4209.

(38) Zhang, J.; Zhao, Y.; Hixson, R.S.; Gray, G.T.; Wang, L.; Utsumi, Hiroyuki S., Takanori, H. Thermal equations of state for titanium obtained by high pressure—temperature diffraction studies. Physical Review B 78 (2008) 054119.

(39) Cremasco, A.; Andrade, P.N.; Contieri, R.J.; Lopes, E.S.N.; Afonso, C.R.M.; Caram, R. Correlations between aging heat treatment, ω phase precipitation and mechanical properties of a cast Ti–Nb alloy. Materials and Design 32 (2011) 2387–2390.

(40) Moffat, D.L, Larbalestier, D.C. The competition between martensite and omega in quenched Ti-Nb alloys. Metallurgical Transactions **19** (1988) 1677.

(41) Brown, A.R.G.; Clark, D.; Eastabrook, J.; Jepson, K.S. The Titanium–Niobium System. Nature 210 (1964) 914–15.

(42) Jaffee, R. I.; Promisel, N. E. The science technology and application of titanium: proceedings of an international conference organized by the Institute of Metals and held at the Royal Festival Hall, London, (1968) Pergamon, Oxford.

(43) Sun, J.; Yao, Q.; Xing, H.; Guo, W.Y. Elastic properties of β, α" and ω metastable phases in Ti–Nb alloy from first-principles. Journal of Physics: Condensed Matter 19 (2007) 486215.

(44) Moffat, D.L.; Kattner, U.R. The pressure-temperature phase diagram of pure titanium. The Stable and Metastable Ti-Nb Phase Diagrams. Metallurgical Transactions A. Volume 19A (1998) 2389-2397.

(45) Bönisch, M.; Calin, M.; Waitz, T.; Panigrahi, A.; Zehetbauer, M.; Gebert, A.; Skrotzki, W.; Eckert, J. Thermal stability and phase transformations of martensitic Ti–Nb alloys. Science and Technology of Advanced Materials 14 (2013) 055004.

(46) Lekka, Ch.E.; Gutierrez Moreno, J.J.; Calin, M. (accepted for publication in the Journal of Physics and Chemistry of Solids).

(47) Gutierrez-Moreno, J.J.; Guo, Y.; Georgarakis, K.; Yavari, A.R.; Evangelakis, G.A.; Lekka, Ch.E. The role of Sn doping in the β-type Ti-25at%Nb alloys: experiment and ab initio calculations. Journal of Alloys and Compounds 615 1 (2014) S676–S679.

(48) S. Kibey, H. Sehitoglu, D.D. Johnson. Energy landscape for martensitic phase transformation in shape memory NiTi. Acta Materialia Volume 57, Issue 5 (2009) 1624-1629.

(49) W.G. Burgers. On the process of transition of the cubic-body-centered modification into the hexagonal-close-packed modification of zirconium. Physica Volume 1, Issues 7–12 (1934) 561–586.

(50) Y.A. Bagariatskii, G.I. Nosova, T.V. Tagunova. Factors in the Formation of Metastable Phases in Titanium-Base Alloys. Soviet physics Doklady 3 (1958) 1014-1018

(51) J.P. Morniroli, M. Gantois. Investigation of the conditions for omega phase formation in Ti-Nb and Ti-Mb alloys. Memoires et etudes scientifiques de la revue de metallurgie. 70 (1973) 831-842

Table I. Space groups, basis vectors and atoms, Ti-xNb compositions (at%), Ti-xNb total and Nb number of atoms as well as the corresponding number k-points for each supercell. In the α'' phase the parameter y is set to 0.1 that is the typical value for the Ti-Nb alloys [51]

Phase	**α' phase**			**ω phase**			**α'' phase**			**β phase**		
Space group	P63/mmc (No. 194)			P6/mmm (No. 191)			Cmcm (No. 63)			lm3̄m (No. 229)		
Basis vectors	$\|\mathbf{a}_1\|=\|\mathbf{a}_2\|=a$; $\mathbf{a}_3=c$ $\alpha=\beta=90°$; $\gamma=120°$			$\|\mathbf{a}_1\|=\|\mathbf{a}_2\|=a$; $\mathbf{a}_3=c$ $\alpha=\beta=90°$; $\gamma=120°$			$\|\mathbf{a}_1\|=a$; $\|\mathbf{a}_2\|=b$; $\mathbf{a}_3=c$ $\alpha=\beta=\gamma=90°$			$\|\mathbf{a}_1\|=\|\mathbf{a}_2\|=\|\mathbf{a}_3\|=a$ $\alpha=\beta=\gamma=90°$		
Basis atoms	(1/3, 2/3, 1/4); (2/3, 1/3, 1/4)			(0, 0, 0); (1/3, 2/3, 1/2) (2/3, 1/3, 1/2)			(0, 0, 0); (1/2, 1/2, 0); (0, y, 0); (0, 1/2+y, 1/2)			(0,0,0)		
Ti-xNb (at%)	**Total atoms**	**Nb atoms**	**k-points**	**Total atoms**	**Nb atoms**	**k-points**	**Total atoms**	**Nb atoms**	**k-points**	**Total atoms**	**Nb atoms**	**k-points**
0.000	2	0	2925	3	0	1098	4	4	2736	1	0	1540
5.556	-	-	-	18	1	756	-	-	-	-	-	-
6.250	16	1	560	-	-	-	16	15	192	16	1	288
8.333	-	-	-	12	1	420	-	-	-	-	-	-
9.375	-	-	-	-	-	-	32	29	96	32	3	242
10.000	10	1	576	-	-	-	-	-	-	-	-	-
11.110	-	-	-	9	1	368	-	-	-	-	-	-
12.500	8	1	576	-	-	-	8	7	432	8	1	286
16.667	6	1	1085	6	1	534	6	5	456	-	-	-
18.750	16	3	560	-	-	-	16	13	192	16	3	288
25.000	4	1	1014	12	3	342	16	12	192	16	4	288
26.000	-	-	-	-	-	-	-	-	-	20	7	428
31.250	-	-	-	-	-	-	-	-	-	16	5	288
33.333	6	2	1085	3	1	1098	-	-	-	-	-	-

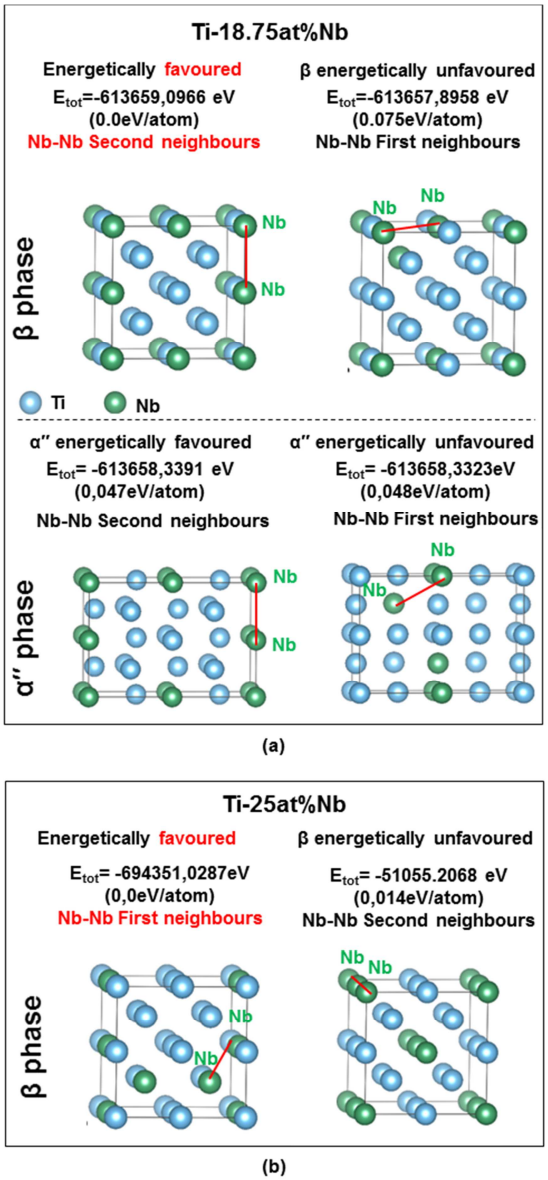

Figure 1. Schematic representation of the different Nb occupation sites within a) Ti-18.75at%Nb for the β and α″ phases and b) β Ti-25at%Nb having Nb-Nb First or Second neighbours. The DEtotvalues/eV/atom are given relatively to the energetically favored phase for each Nb composition in parenthesis. Blue and green spheres correspond to the Ti and Nb atoms.

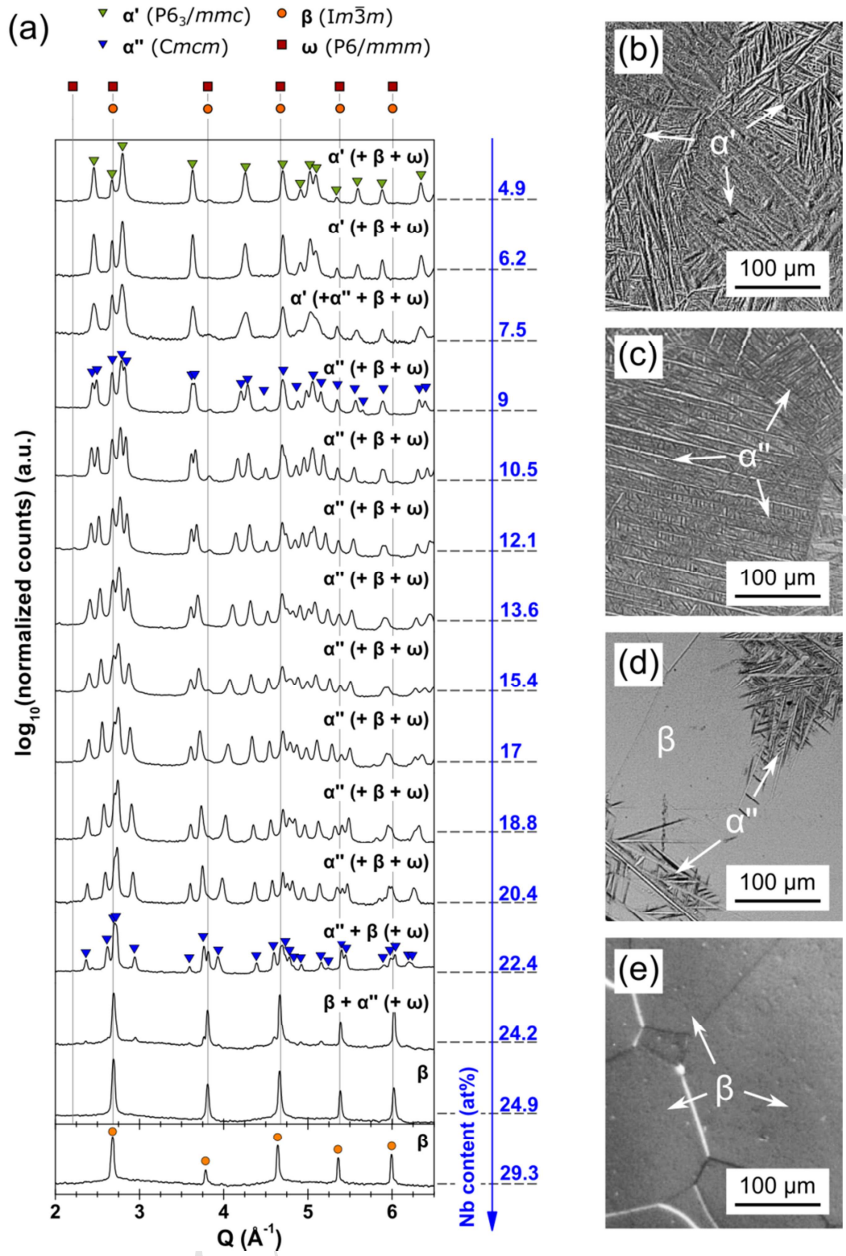

Fig. 2. (a) X-ray diffractograms and (b-e) LM images of homogenized and water quenched (HQ) Ti-Nb alloys. The alloy compositions corresponding to (b-e) are (b) Ti-7.5Nb (at%), (c) Ti-20.4Nb (at%), (d) Ti-24.2Nb (at%) and (e) Ti-29.3Nb (at%).

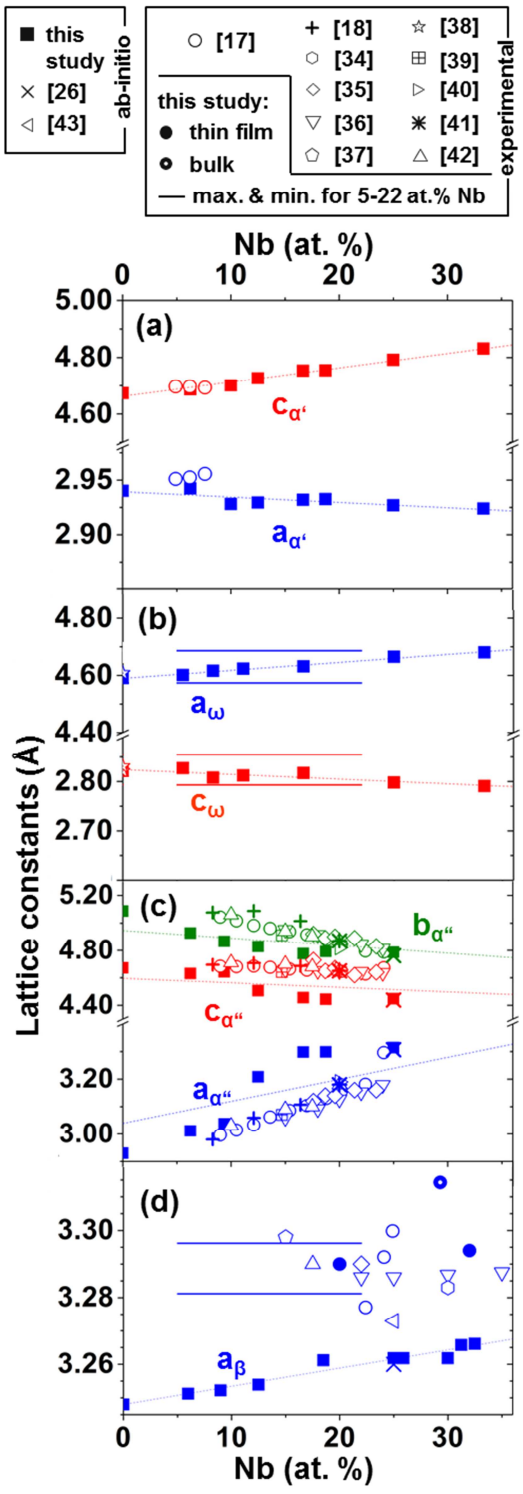

Fig. 3. Lattice parameters of (a) α′, (b) ω, (c) α″ and (d) β-phase as a function of Nb content. Dotted lines represent linear fits through the ab-initio results of the present study.

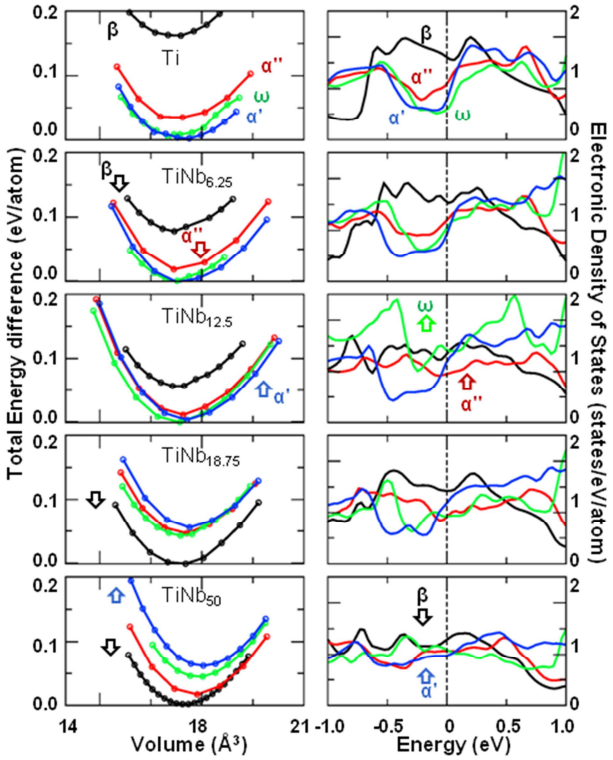

Fig. 4. Total energy per atom under hydrostatic pressure as a function of the unit cell volume (first column) versus EDOS (second column) for the pure Ti and selected Ti-xNb (x=6.25, 12.5, 18.75, 50 at%) alloys. Black, red, green and blue lines/arrows stand for the β, α", ω and α'-phases, respectively while the up/down arrows denote the increasing/decreasing trend of the corresponding phase's total energy difference or the EDOS occupation at E_F.

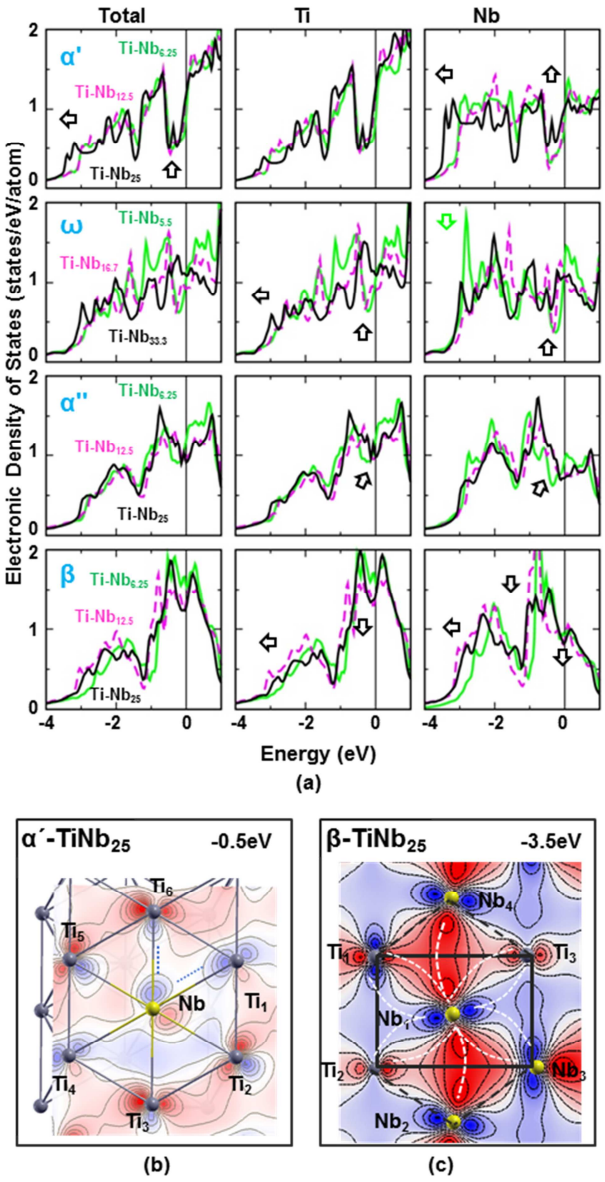

Fig. 5. (a) Total and partial Ti and Nb EDOS for the α', ω, α" and β phases. From the top to the bottom the rows belong to α', ω, α" and β. The Nb content increases with the line color in the order of green, magenta and black. (b,c) Contour plots of the electronic wavefunction at the Γ k-point (b) of α'-Ti-25Nb (at%) or -0.5eV on $(0001)_{\alpha'}$ and (c) of β-Ti-25Nb (at%) for -3.5eV on $(110)_{\beta}$. Yellow and grey balls represent Nb and Ti atoms, respectively, while red and blue areas for the negative and positive charge of the wavefunction.

Highlights:

- α', α", β and ω-phases in Ti-Nb are studied by ab-initio and experimental methods.
- The Ti-Nb favoured stability is related to its lowest total energy.
- The electronic lowest occupation/energy values link to the favoured phase
- At high Nb content, antibonding Nb p – Ti d hybridizations destabilize α´ and ω.
- Directional strong bonding between Ti d - Nb d stabilize the β-phase.